Sustainable Chemistry and Pharmacy 32 (2023) 101017

Contents lists available at ScienceDirect

Sustainable Chemistry and Pharmacy

journal homepage: www.elsevier.com/locate/scp

Efficient mercury removal from water by using modified natural zeolites and comparison to commercial adsorbents

Vassilis J. Inglezakis [a, *], Aliya Kudarova [b], Almira Guney [d], Nurassyl Kinayat [c, d], Zhandos Tauanov [e, f]

[a] Department of Chemical & Process Engineering, University of Strathclyde, Glasgow, UK
[b] School of Engineering & Digital Sciences, Nazarbayev University, Nur-Sultan, Kazakhstan
[c] Department of Chemical & Materials Engineering, School of Engineering & Digital Sciences, Nazarbayev University, Nur-Sultan, Kazakhstan
[d] The Environment & Resource Efficiency Cluster (EREC), Nazarbayev University, Nur-Sultan, Kazakhstan
[e] Faculty of Chemistry & Chemical Technology, al-Farabi Kazakh National University, Almaty, Kazakhstan
[f] LLP "Scientific Production Technical Center "Zhalyn", Almaty, Kazakhstan

ARTICLE INFO

Handling Editor: Klaus Kümmerer

Keywords:
Natural zeolite
Nanocomposites
Silver nanoparticles
Silver oxide
Mercury removal

ABSTRACT

The reduction of mercury use in industrial activities and its elimination from waste streams is of great importance to the circular economy approach. In this study a natural zeolite was impregnated with silver to derive Ag^+, Ag_2O and Ag^0 forms. The natural and Ag-zeolites were effectively used for the removal of mercury from $Hg(NO_3)_2$ and $HgCl_2$ aqueous solutions. Kinetic experiments, aqueous phase speciation modeling and post-sorption characterizations were used to interpret the sorption behavior of the zeolites. Natural zeolite is effective in removing mercury from $Hg(NO_3)_2$ solutions but sorption is negligible from $HgCl_2$ solutions. Silver modification transformed the natural zeolite into an effective nanocomposite sorbent for mercury removal from $HgCl_2$ solutions, the effectiveness being affected by the Ag form. However, Ag modification had no effect on the removal from $Hg(NO_3)_2$ solutions. These results demonstrate the strong interplay between ion exchange, surface Ag–Hg reactions and the aqueous phase Hg speciation which was further supported by complementary experiments with iodide under the same conditions. For comparison, Hg removal by commercial adsorbents, namely an activated carbon, a cation exchange resin and synthetic zeolite Y is presented. The results demonstrate that natural zeolite and Ag^0 form are effective adsorbents performing better than commercial ion exchangers and are comparable to activated carbon. The use of abundant, cheap, environmental-friendly and easy to modify natural zeolite is an attractive alternative to commercial and other unsustainable and difficult to synthesize adsorbent materials.

1. Introduction

The removal of hazardous chemicals from products, processes and wastes can facilitate the reuse and recycling of materials, promoting circularity with significant environmental and social gains. The presence of toxic substances in wastewater combined to the limited efficiency of wastewater treatment plants represent a significant barrier towards circularity as the produced water has limited uses and the waste sludge may be unsuitable for recycling on land.

* Corresponding author.
E-mail address: vasileios.inglezakis@strath.ac.uk (V.J. Inglezakis).

https://doi.org/10.1016/j.scp.2023.101017
Received 8 December 2022; Received in revised form 26 January 2023; Accepted 28 January 2023
Available online 31 January 2023

Contamination of natural waters with mercury in its organic and inorganic forms is a serious global environmental problem. Although mercury is emitted by natural sources, such as volcanoes and forest fires the major sources are anthropogenic (Gworek et al., 2016; Siva et al., 2015; Kabiri et al., 2015). The anthropogenic sources are responsible for the release of more than 2220 tons of mercury in air in 2015 mainly coming from small-scale gold mining (38%) and coal combustion (AMAP/UN Environment Expert Group, 2018). Organic forms of mercury produced via microbial activity are particularly toxic and accumulate into the food chain. Mercury compounds in general are more toxic than compounds of any other non-radioactive heavy element (Beckers and Rinklebe, 2017a). Among others, mercury may affect the neurological and mental functions, causes dizziness, irritability, anorexia, hypertension, tachycardia and memory loss and affects the digestive and renal systems (Yorifuji et al., 2010, 2011; Kamensky et al., 2019). On August 16th, 2017, the Minamata Convention on Mercury was ratified by more than 50 parties to the treaty (Esdaile and Chalker, 2018). By the time the treaty enters into force, new Hg mining will be banned and any Hg mines in operation must be closed within 15 years from that date (Beckers and Rinklebe, 2017b).

There are several methods available for the removal of mercury from water, such as membrane separation, precipitation, adsorption, ion exchange and bioremediation (Azimi et al., 2017; Wang et al., 2020a). Adsorption is the most common, simple, effective and low-cost method and various materials have been used for mercury removal from water such as activated carbons (Saha et al., 2016), fumed silica (Inglezakis et al., 2021a), synthetic zeolites (Tauanov et al., 2018, 2019; Bahiraei and Behin, 2020), resins (De Clercq, 2012) and several silver forms of alumina, zeolites, graphene (Tauanov et al., 2018; Sumesh et al., 2011; Qu et al., 2017) and synthetic polymers (Ge and Hua, 2016; Wang et al., 2014; Tikoalu et al., 2020; Crockett et al., 2016; Baimenov et al., 2020). A detailed review on mercury removal methods and materials was published by Wang et al. (2020b).

Natural zeolites are low cost, non-toxic and environmentally friendly adsorbents that can easily modified to derive adsorbents suitable for a variety of applications. Clinoptilolite is the most used natural zeolites in the field of water treatment owing to its abundance, porosity, stability and ion exchange properties (Yu et al., 2018; Golubeva and Ul'yanova, 2015; Inglezakis et al., 2002; Kuntubek et al., 2020). Compared to synthetic zeolites and other materials clinoptilolite is cost-effective and suitable for large-scale water/wastewater applications. There are several studies on the removal of mercury species from water by using natural and synthetic zeolites. For instance, Campbell et al. studied the uptake of Hg^{2+} from aqueous solutions by 11 different natural zeolites (Campbell et al., 2006a). In another study, natural and Na^+-exchanged clinoptilolite were used to remove Hg^{2+} from $Hg(CH_3COO)_2$ solutions (Misaelides and Godelitsas, 1995a). Tauanov et al. (2019) used synthetic sodalite impregnated with Ag^0 nanoparticles to remove mercury from $HgCl_2$ solutions. Table 1 summarizes the published studies on the topic of this paper.

As it is evident, there are relatively few studies on the use of unmodified zeolites for mercury removal from water and, to the best of our knowledge, none on Ag-modified clinoptilolite. Furthermore, there are no studies on the effect of co-existing anions with the exception of few data presented by Tauanov et al. (2019) who used synthetic sodalite impregnated with Ag^0 nanoparticles and studied the removal of mercury in $HgCl_2$, $Hg(NO_3)_2$, $HgSO_4$ and $HgAc_2$ solutions. Another important observation drawn from the published studies is the absence of comprehensive research on different Ag-modified natural zeolites for mercury removal from water, the effect of the water phase speciation and the mechanisms involved.

In our previous work Ag_2O and Ag^0 forms of the same natural zeolite were used for the removal of iodide from water (Inglezakis et al., 2020a). In this work we present the results on mercury removal by using similar silver forms for the removal of various forms of mercury from water. The amount of silver used for the zeolite modification was kept small to reduce the associated costs and environmental footprint. Three different silver forms of the zeolite were synthesized; ion exchanged containing silver ions (Ag^+) and two nanocomposites containing silver oxide (Ag_2O) and metallic silver (Ag^0) nanoparticles. Kinetic and equilibrium data, materials characterization and aqueous phase mercury speciation were used to derive plausible mercury uptake mechanisms. An experiment with iodide removal was repeated to provide further support for our hypothesis on the surface interactions.

2. Materials & methods

2.1. Natural zeolites and Ag-forms synthesis

The following chemicals were used: NaCl (≥99.0%), KI (≥99.0%), $AgNO_3$ (>99.9%), $NaBH_4$ (99%) 99.8%), $Hg(NO_3)_2$ (>99%), and HgCl (>99%). Ultrapure (UP) water obtained by Millipore filtration was used for the preparation of all solutions. The natural zeolite of content of 80% clinoptilolite (NZU) was obtained from the company "Transcarpathian zeolitic factory" (Khust district, Ukraine) The activated carbon (GUNT), strongly acidic cation exchange resin (H^+ form) (Merck) and zeolite Y (Sigma-Aldrich) were washed with deionized water, dried and stored in desiccator.

The as-received material was sieved on the vibrating sieve AS200 (Retsch, GmbH) to obtain the 0.8–1.4 mm fraction, thoroughly washed and dried at 150 °C for 24 h (NZU). The Na-form of the zeolite was preapred by adding 100 g of NZU to 1 M NaCl at 60 °C. The NaCl solution was replaced daily for 7 days and at the end of this period the zeolite was washed, oven-dried at 60 °C for 24h and stored in a desiccator (Na-NZU) (Lihareva et al., 2010). The removal of excess Cl-ions was confirmed by adding $AgNO_3$ in the supernatant solution after washing and the absence of AgCl precipitate. The Ag ion exchanged form of the zeolite (Ag^+@NZU) was prepared by placing 100g of Na-NZU into 250 ml of 0.1 M $AgNO_3$ solution at ambient temperature without agitation for 24h under dark conditions. The solids were thoroughly washed with deionized water, oven-dried at 60 °C for 24h and placed in a desiccator. Dark conditions throughout the synthesis and low drying temperature and were used to minimize the oxidation of Ag^+ on the zeolite surface. The oxidized Ag form of the zeolite (Ag_2O@NZU) was prepared by further heating 70g of Ag^+@NZU in an oven for 24h under 150 °C. The metallic Ag form of the zeolite (Ag^0@NZU) was prepared by adding 0.5 M $NaBH_4$ solution in a beaker containing 35 g of Ag_2O@NZU until the solids are fully immersed into the solution (Mulfinger et al., 2007). The beaker was immersed in an ice bath with

Table 1
Natural and synthetic zeolites used for the removal of mercury from water.

Zeolite	Initial Hg concentration (ppm)	Salt used	Initial pH	Adsorption capacity (mg/g)	Ref.
Natural zeolites					
Na-Clinoptilolite Ag^+-Clinoptilolite Ag_2O@Clinoptilolite Ag^0@Clinoptilolite	200	$Hg(NO_3)_2$ $HgCl_2$	2.5	9–26	This work
Clinoptilolite Philipsite Mordernite Analcime Stilbite Na-Chabazite Laumontite	0.1–5	$Hg(NO_3)_2$	–	–	Campbell et al. (2006b)
Na-Heulandite Na-Clinoptilolite	10–500	$Hg(CH_3COO)_2$	2.5	16.3–43	Misaelides and Godelitsas (1995b)
Clinoptilolite	0.47	–	–	58–121	Chojnacki et al. (2004)
Clinoptilolite Fe-Clinoptilolite	92–2450	$Hg(NO_3)_2$	2.09–2.3	56–108	Ugrina et al. (2020)
Clinoptilolite HDTMABr-clinoptilolite	25–800	–	2–10	70–170	Shirzadi and Nezamzadeh-Ejhieh (2017)
Natural zeolite Dithizone-Natural zeolite	5	$HgCl_2$	3–9	1.6–2.6	Mudasir et al. (2016)
Ca-clinoptilolite Cetylpyridinium bromide (CPB) modified clinoptilolite	0.1–5	$Hg(NO_3)_2$	5.94–6.09	0.05–0.40	Liu et al. (2016)
Mordenite	10	$HgCl_2$	N/A	0.14–0.44	Prasetya et al. (2020)
Clinoptilolite	0.05–2.4	$HgCl_2$	5.5–6.5	0.001–0.24	Oliveira et al. (2020)
Magnetic mordenite	700	$Hg(NO_3)_2$	N/A	16.7–26.2	Andrade et al. (2019)
Synthetic zeolites					
Linde Type A CFA derived zeolite	10	$HgCl_2$	2.5	0.08–0.31	Attari et al. (2017)
ZnS-Zeolite NaA Zeolite NaA	10–470	$HgCl_2$	2–7	0.3–553	Li et al. (2021)
Muscovite-P-zeolite	50–350	Hg(II)	4	117	Salam et al. (2020)
Na-A ZSM-5	2–50	$HgCl_2$	2–10	32.3–45.4	Alijani et al. (2015a)
β-Zeolite Zeolite-Y Mordenite	5	$HgSO_4$	3–10	1.25	Murthy et al. (2013)
Thiol-functionalized B/MCM-41	50–1500	$Hg(NO_3)_2$	1–4	798	Fardmousavi and Faghihian (2014)
Sulfur-zeolite	10–200	$HgCl_2$	1–7	4.4–12.1	Fang et al. (2018)
NaP MnO_2@NaP	20	$HgCl_2$	7	103–581	Bahiraei and Behin (2020)
Faujasite	0.5 (ppb)	–	4.5	–	Somerset et al. (2008)
Na-A	0.3	–	2–10	–	Azizi et al. (2013)
NaP1	0.02–1.5	$Hg(NO_3)_2$	4.5	0.23	Sánchez-Hernández et al. (2018)
Na-A, Na–Y	3–100	$HgCl_2$	7–7.3	0.014–3.9	Hernandez-Tamargo et al. (2021a)
Na-A Na-X 13X 4A Ag–Na-X	13.2–575	$HgCl_2$	5–6	0.12–5.1	Czarna et al. (2018)
Sodalite Ag^0@Sodalite Alalcime Ag^0@Analcime	10–500	$HgCl_2$	2	4–22.3	(Tauanov et al., 2018, 2019, 2020)

a thermostat at 3 °C for 1h. Then the zeolites were washed with deionized water to a neutral pH, oven-dried at 60 °C for 8h and placed in a desiccator.

2.2. Materials characterization

The chemical composition of the natural and Ag-modified zeolites was studied by X–ray fluorescence (XRF) on an Axios Max (PANalytical, Malvern). The samples were pelletized by using 99.5% boric acid in a ratio of 1/3 and the measurements were per-

formed in vacuum at 40–50 kV. A PerkinElmer STA 6000 was used for the thermal analysis under nitrogen atmosphere with a heating rate 10 °C•min^{-1} and temperature range from 50 to 950 °C. The X-ray diffraction (XRD) was performed on a Rigaku (SmartLab® X-ray) with Cu Kα radiation source (λ = 1.540056 Å) at a scan rate of 0.02° θ•s^{-1} in the 2θ range of 5–90°. The surface of the materials was studied by Scanning Electron Microscopy (SEM) using a JEOL 6380 LV scanning electron microscope equipped with a backscattered electron detector at 20–30 kV. Mapping analyses were carried out using a Si (Li) energy-dispersive x-ray spectrometer (Oxford Instruments) connected to SEM. A high-resolution JEM-2100 LaB_6 transmission electron microscope (HRTEM, JEOL) operating at 200 kV WSAS used for the detection of nanoparticles. The porosity and surface area were determined by using low-temperature nitrogen adsorption on an Autosorb-1 (Quantachrome Instruments). The particle size distribution (PSD) of the commercial adsorbents was done on a Malvern Mastersizer 3000 particle size analyzer.

2.3. Adsorption experiments

The adsorption experiments were done in batch mode by bringing in contact 1.5 g of adsorbent samples with 150 mL of 200 ppm mercury ($HgCl_2$ or $Hg(NO_3)_2$) or iodide (KI) solutions with initial pH adjustment by using HNO_3 at 2.5 and room temperature. Solution samples were taken after specified time and diluted by using UP water before analysis. The mercury concentration was measured by pyrolysis technique on a RA-915 M mercury analyzer (Lumex). The iodide concentration was measured by using a UV–Vis spectrophotometer (Evolution 300, Thermo Fisher) at 225 nm wavelength. In all experiments the total sampling volume was lower than 5%. The solid phase loading (q_t, mg/g) was calculated as follows:

$$q_t = \frac{C_o - C_t}{m} \times V \tag{1}$$

where C_o and C_t are the initial and final solutions concentrations (mg/L), respectively, V the volume of solution (L), and m is the initial weight of the zeolites (g). The solid phase loading is based on the initial weight of the zeolite (before adsorption) and the term "content" (c_t, mg/g) is used in this paper to differentiate the amount of mercury adsorbed per total weight of the zeolite (after the adsorption):

$$c_t = \frac{q_t}{1 + \left(\frac{q_t}{1000}\right)}$$

3. Results and discussion

3.1. Materials characterization

The XRD patterns of all samples showed the clinoptilolite characteristic peaks at 9.87°, 22.5° and 30.2° and a peak at 26.7° attributed to quartz (Fig. 1) (Stylianou et al., 2018a). The Ag^+@NZU and Ag_2O@NZU XRD patters showed the same peaks and thus there is no evidence of other phases formation. The mineralogical composition of the Ag^0@NZU sample is shown in Fig. 1. The observed peaks at 38.18°, 44.3°, 64.6°, and 77.5° are characteristic of metallic Ag^0.

Nitrogen porosimetry showed the characteristic to mesoporous materials hysteresis loop in the nitrogen adsorption–desorption isotherm for all samples is characteristic of mesoporous materials (Fig. 2). Furthermore, the Na and Ag modification had no signifi-

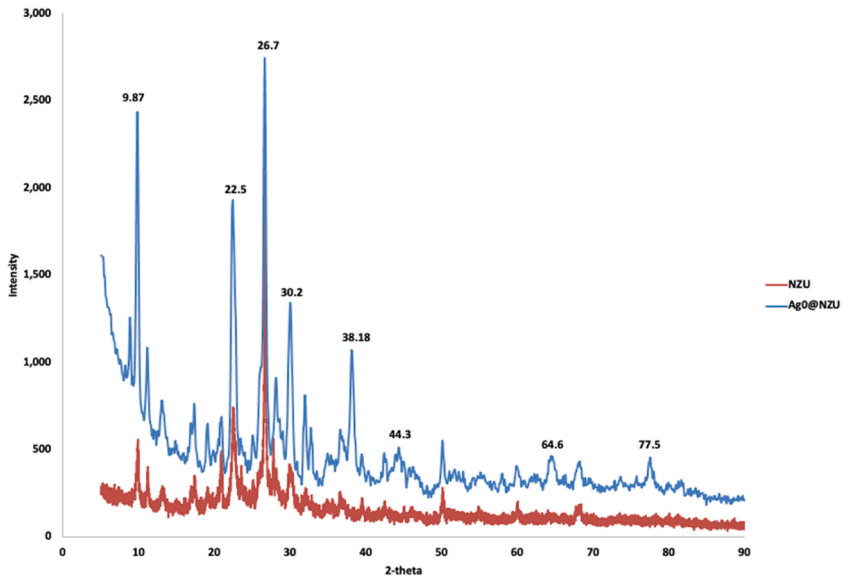

Fig. 1. XRD pattern of NZU and Ag^0@NZU.

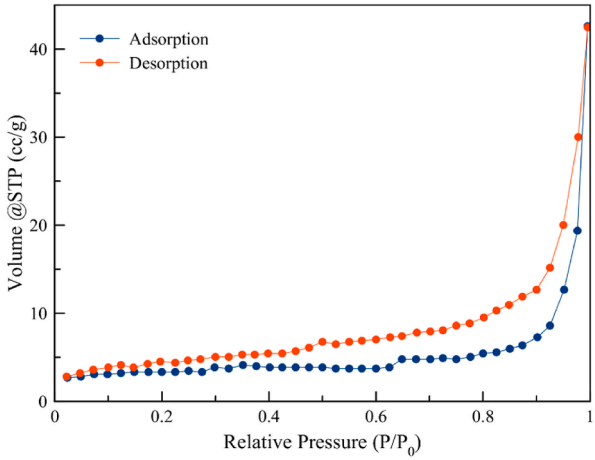

Fig. 2. Adsorption-desorption isotherm for NZU.

cant effect on the porous structure of the zeolites (Table 2). The surface area of the zeolites is relatively small but within the range for other samples (Stylianou et al., 2018b).

The thermogravimetric analysis of all zeolites showed no significant differences between the samples (Fig. 3). There is a continuous weight loss of approximately 10% to 900 °C due to the loss of adsorbed and structural water, which is typical for clinoptilolite (Bahiraei and Behin, 2020; Stylianou et al., 2018c).

The elemental XRF analysis of all samples is shown in Table 3. Although zeolite is dried before experiments, and stored in a desiccator some crystalline water remains in the structure. The content measured by XRF (and EDX) does not take into account the water and thus the actual amount of elements present in the zeolite structure is somewhat overestimated. In total 15 samples were analyzed before and after the adsorption and taking into account the semi-quantitative nature of XRF analysis the results are satisfactory. There are three notable outliers, the high Fe content of Na-NZU, the low Fe content of Ag^{+}@NZU and high Ag content of Ag^{0}@NZU all before mercury sorption, which are considered analytical errors as the rest 12 samples show very consistent results for both elements. It is relevant to mention that Ag dissolution in the solutions was found to be negligible (Inglezakis et al., 2020b). The elemental composition is within the literature ranges for all elements (Stylianou et al., 2018b). As expected, Ag is observed on the modified samples with an Ag content of about 2.5%. After adsorption Hg and I are observed on the zeolite samples, a result which is further discussed in Section 3.2.

Table 2
BET/BJH results.

Sample	Surface area (BET, m^2/g)	Total pore volume (BJH, cm^3/g)	Average pore size (BJH, nm)
NZU	12.6	0.03	5.82
Na-NZU	12.5	0.03	2.98
Ag^{+}@NZU	15.4	0.08	3.72
Ag_2O@NZU	12.8	0.07	3.94
Ag^{0}@NZU	13.2	0.09	3.72

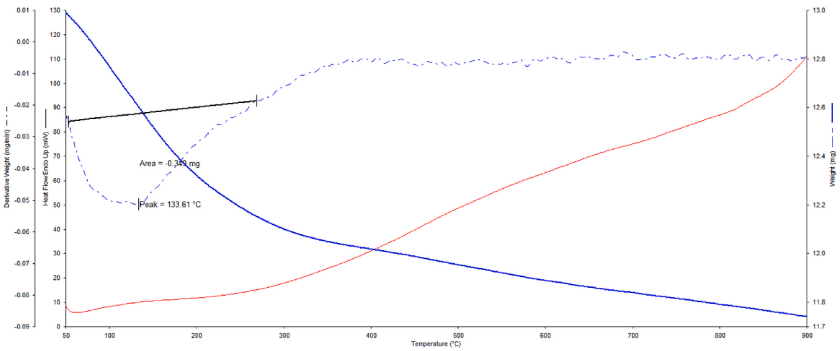

Fig. 3. TG/DTA/DSC analysis of Na-NZU sample.

Table 3
The XRF analysis results (% *w/w*).

NZU	Na-NZU	Ag^+@NZU	Ag_2O@NZU	Ag^0@NZU
Before sorption				
Na_2O	2.28	0.59	0.53	0.79
MgO	0.27	0.18	0.17	0.16
Al_2O_3	12.68	10.92	10.82	10.31
SiO_2	70.39	78.74	78.32	73.18
K_2O	1.36	2.63	2.69	2.98
CaO	0.31	0.83	0.91	1.21
Fe_2O_3	8.05	0.21	2.13	3.55
Ag_2O	0.00	3.08	2.80	6.81
Others	4.67	2.83	1.63	1.00
$HgCl_2$ experiment (after sorption)				
Na_2O	0.45	0.47	0.44	0.62
MgO	0.19	0.24	0.17	0.19
Al_2O_3	11.35	11.17	11.11	11.29
SiO_2	81.39	76.87	77.27	76.26
K_2O	2.65	2.80	2.80	2.67
CaO	0.85	0.86	0.90	0.84
Fe_2O_3	1.98	1.94	1.92	1.74
Ag_2O	0.00	2.48	2.49	2.64
HgO	0.1	1.91	1.87	2.78
Others	1.06	1.26	1.06	0.98
$Hg(NO_3)_2$ experiment (after sorption)				
Na_2O	0.47	0.40	0.31	0.38
MgO	0.15	0.14	0.11	0.131
Al_2O_3	11.35	10.39	10.24	10.19
SiO_2	81.39	77.95	76.83	77.00
K_2O	2.65	2.48	2.43	2.48
CaO	0.85	0.83	0.87	0.85
Fe_2O_3	1.98	1.81	2.12	2.00
Ag_2O	0.00	2.85	3.42	3.05
HgO	3.29	2.70	3.05	2.89
Others	1.15	0.46	0.62	1.03
KI experiment				
Na_2O	–	0.52	0.51	0.67
MgO	–	0.16	0.15	0.21
Al_2O_3	–	10.89	10.47	11.22
SiO_2	–	78.02	78.01	76.38
K_2O	–	3.29	3.42	3.63
CaO	–	0.79	0.83	0.89
Fe_2O_3	–	2.06	2.08	1.96
Ag_2O	–	2.10	2.28	2.58
I	–	0.91	1.04	1.14
Others	–	1.26	1.21	1.31

TEM imaging clearly showed that nanoparticles were formed on all zeolites (Fig. 4). The particles are mostly spherical with sizes ranging from 4 to 40 nm and those of the Ag^0@NZU were about 18 nm as estimated by using Scherrer equation, within the range found by TEM imaging.

As is evident, nanoparticles are formed in all samples and while this is expected in the case of Ag^0@NZU the explanation is less clear in the case of the Ag^+@NZU and Ag_2O@NZU. Our hypothesis is that silver clusters and reduction are responsible for the nanoparticles formation in these samples. Sub-nanometer silver clusters, denoted as Ag_m^{n+} ($n < 10$), represent the link between atomic and conventional nanoparticles and differ strongly from conventional nanoparticles (El-Roz et al., 2018; Coutiño-Gonzalez et al., 2017a). The clusters are not stable and tend to aggregate irreversibly into larger nanoparticles. Zeolites have been proven to be an ideal scaffold as the zeolite frameworks possess the appropriate cation-exchange properties to uptake Ag^+ and molecular-sized pores and cages to contain Ag-clusters (Coutiño-Gonzalez et al., 2017b). Another advantage of zeolites is that the negative charge of the structure and the coordinating properties of the oxygen atoms further stabilizate the metal clusters (De Cremer et al., 2009a). Reduction of silver clusters and nanoparticles can be achieved by several methods but the conditions used and the characterization methods may affect the formation of silver clusters and nanoparticles. The photoreduction of Ag^+ and formation of Ag_m^{n+} clusters during ion

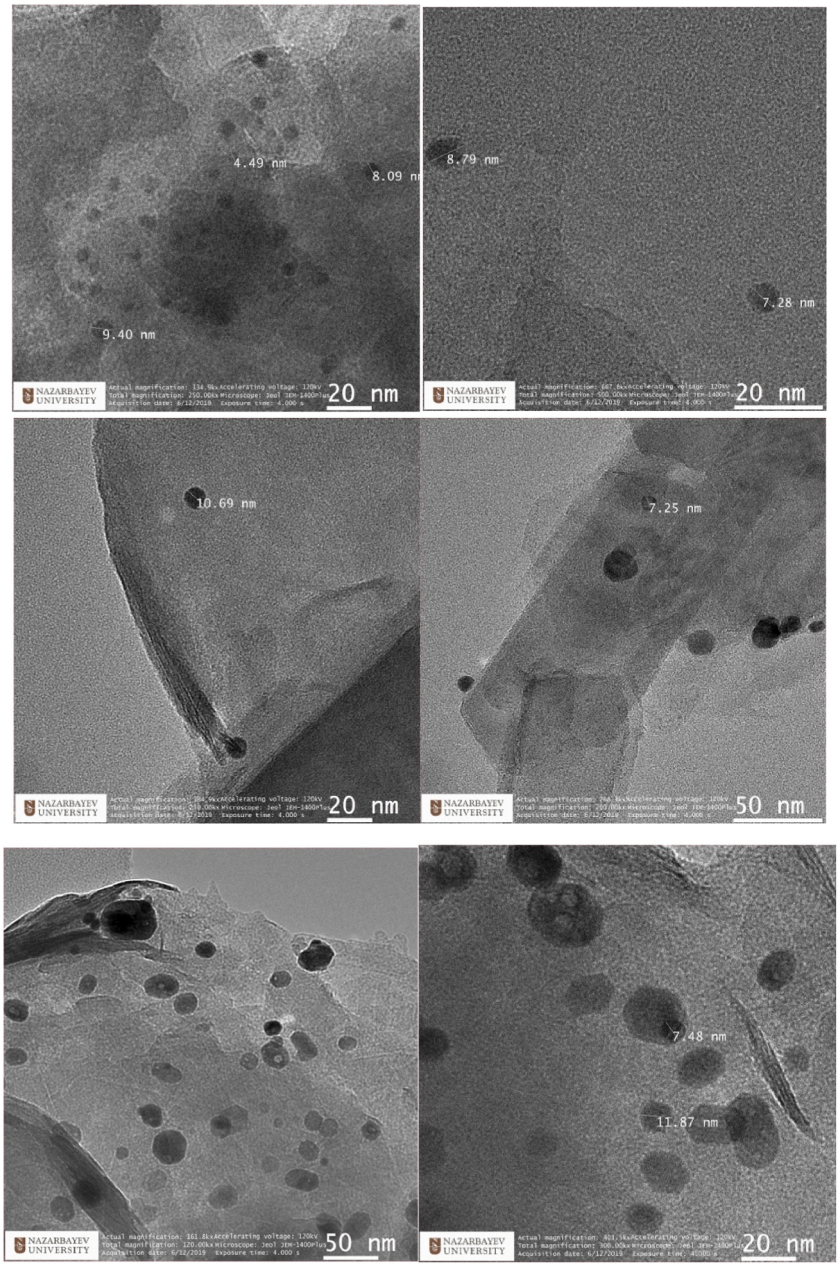

Fig. 4. TEM images from top to bottom; Ag^{+}@NZU, Ag_2O@NZU and Ag^0@NZU.

exchange experiments has been reported for ZSM-5, NaX and NaY zeolites (Tarach et al., 2014). El-Roz et al. used FAU-type zeolite as a scaffold and photocatalytic reduction to grow silver sub-nanometer Ag_m^{n+} clusters (El-Roz et al., 2018). FAU Ag^{+}-exchanged zeolite was also studied by Taiji and Isobe (Taiji et al., 2018). Ag^{+}-exchanged zeolite was irradiated with X-rays to improve its photoluminescence properties. The authors report that silver clusters and/or silver nanoparticles were developed from Ag^{+}, possibly through redox reactions in the zeolite structure during X-ray irradiation. Also, small dots were observed by TEM possibly being Ag^0 particles or oxidized particles such as Ag_2O that formed in air but due to the very small size they didn't show any XRD peaks. Autoreduction of several zeolites has been studied at high temperatures (450–500 °C) in the presence of air (Chebbi et al., 2017; De Cremer et al., 2009b). There is no agreement on the formation of Ag^0 however studies showed the formation of silver clusters. Aspromonte et al. studied Ag-exchanged mordenite prepared in dark and then calcined at 500 °C in O_2 environment (Aspromonte et al., 2013). The results showed isolated Ag^{+}, Ag_m^{n+} cationic clusters and Ag_2O particles. Liu et al. used natural chabazite to develop Ag^0 nanoparticles from Ag^{+} form by calcination at 400 °C in Ar environment (Liu et al., 2011). Under thermal treatment Ag^{+} is partially reduced to silver clusters Ag_m^{n+} and then to Ag^0 by reductants. Silver was impregnated into mordenites and then reduced under heat in hydrogen to Ag^0 nanoparticles and clusters (Gurin et al., 2005).

Discrepancies between XRD and TEM data are not rare and originate from the conditions applied during analysis; in TEM analysis vacuum is applied on the top of intense irradiation while XRD analysis is done under ambient pressure with less intense and focused radiation (Altantzis et al., 2016a). As is known, some zeolites are sensitive to radiation, especially those that with low Si/Al ratio such as FAU zeolites (Altantzis et al., 2016b). However, clinoptilolite has of the highest Si/Al ratio of 4–5.7 compared to other zeolites (Moshoeshoe et al., 2017). Also, reduction of Ag^+ and agglomeration of nanoparticles during TEM measurements is possible. Chebbi et al. (2017) analyzed zeolite Y (Si/Al = 2.5) with a high content of Ag (22.8%) and detected small (1–5 nm) Ag^0 nanoparticles following the exposure to TEM beam. XRD didn't detect any such particles and the authors concluded that most of these nanoparticles were formed during TEM analysis. In the same work in zeolite MOR (Si/Al = 10) with 7.3% Ag aggregated forms of metallic silver (20–30 nm) were also detected due to coalescence phenomena during TEM measurement. Flores-Lopez et al. (Flores-López et al., 2012) studied chabazite and the formation of silver nanoparticles was achieved by thermal annealing in air at 400 °C. The XRD pattern showed no silver peaks and the authors argue that nanoparticles must be smaller than the limit detection of XRD. However, silver content was high enough (18.57%) and TEM analysis showed Ag^0 nanoparticles of sizes in the range of 2–20 nm.

3.2. Sorption kinetics

The kinetics results are shown in Figs. 5 and 6 and as is evident that Na-modified clinoptilolite is an effective sorbent the Ag modification has no effect on the removal of mercury from $Hg(NO_3)_2$ solutions. However, in $HgCl_2$ solutions Na-modified clinoptilolite shows no affinity for mercury and silver forms are effective following the order $Ag^0 > Ag_2O > Ag^+$. Na-modified clinoptilolite shows no affinity for iodide as well, however the Ag forms effectiveness is reversed as shown in Fig. 7. Clearly, the aqueous phase speciation and the surface interactions govern the sorption mechanisms.

XRD analysis after the removal of mercury showed no formation of additional phases and are not presented here. This can be explained by the masking of other phases caused by the complex XRD pattern of the substrate. In the Ag^0@NZU sample the Ag^0 peaks disappeared, a result of combined oxidation by mercury or iodide and the dissolved oxygen in the water. XRF results (Table 3) clearly show the presence of Hg and I on the samples and their amounts follow the trends observed in the removal experiments. The TEM analysis of the samples after adsorption showed smaller in number and bigger in size nanoparticles and dark areas presumably a result of the reduction of silver and the formation of other compounds on the surface (Figs. 8 and 9).

3.3. Mechanisms and surface interactions

The speciation of mercury solutions is shown in Fig. 10. The graphs were created by using Medusa software for 200 and 50 ppm Hg^{2+} concentration at 25 °C. The initial pH of the solutions is 2.5 and increases over time along with a decrease of total Hg^{2+} concentration. Therefore, the speciation changes over time and the major difference is the absence of HgO precipitate in lower total Hg^{2+} concentration. Nevertheless, throughout the experiments precipitation was not observed.

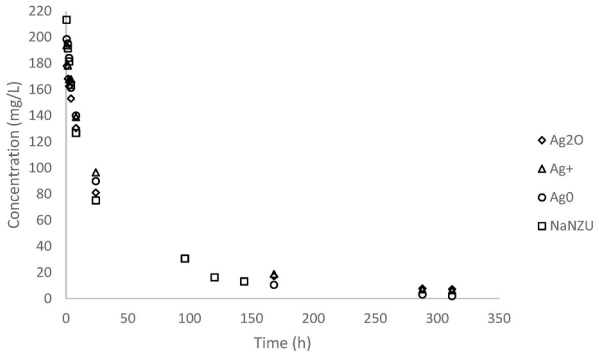

Fig. 5. Removal of mercury by zeolites from nitrate solutions.

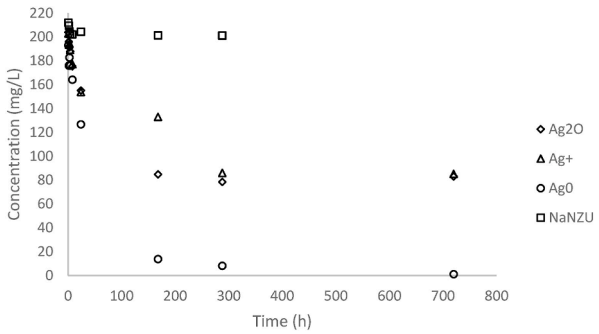

Fig. 6. Removal of mercury by zeolites from chloride solutions.

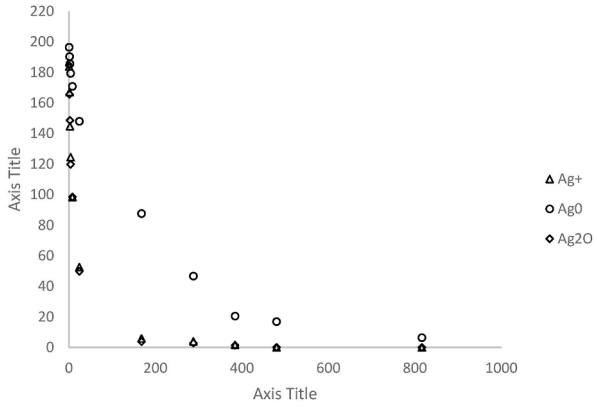

Fig. 7. Removal of iodide by Ag-modified zeolites.

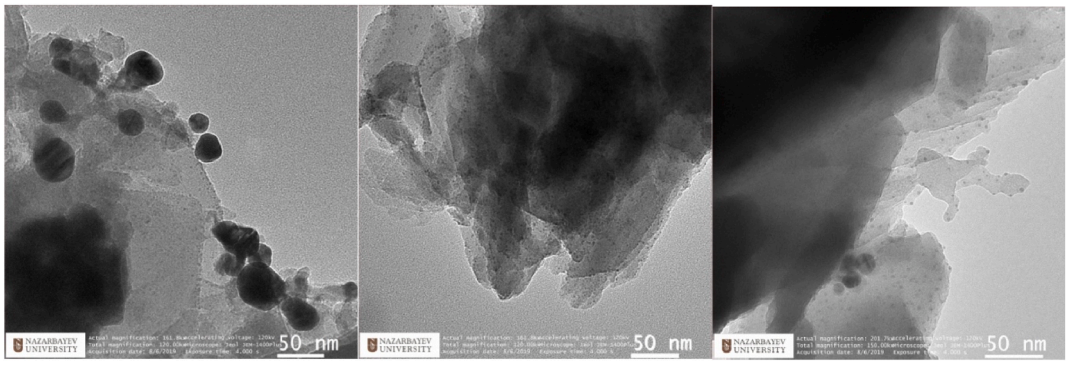

Fig. 8. TEM images after interaction with $Hg(NO_3)_2$ solution from left to right; Ag^+@NZU, Ag_2O@NZU and Ag^0@NZU.

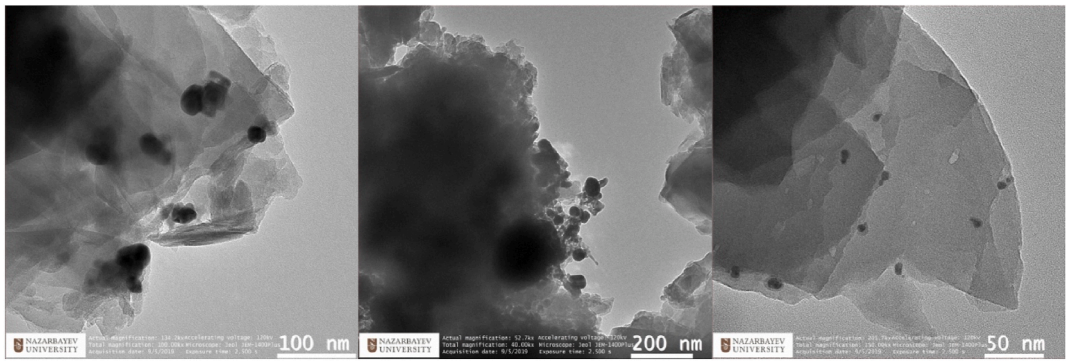

Fig. 9. TEM images after interaction with $HgCl_2$ solution from left to right; Ag^+@NZU, Ag_2O@NZU and Ag^0@NZU.

In $Hg(NO_3)_2$ solutions free Hg^{2+} and $HgOH^+$ ions are available and thus ion exchange with Na^+ ions from the solid phase is possible as the performance of Na-NZU demonstrates. In the presence of Ag^0 the following reactions can take place (Inglezakis et al., 2020c, 2021b):

$$4Ag^0 + O_2 \rightarrow 2Ag_2O \quad (1)$$

$$Ag_2O + 2H^+ \rightarrow 2Ag^+ + H_2O \quad (2)$$

$$Hg^{2+} + 2\,Ag^0 \rightarrow Hg^0 + 2\,Ag^+ \quad (3)$$

$$0.9Hg^0 + 1.1Ag^0 \rightarrow Ag_{1.1}Hg_{0.9} \quad (4)$$

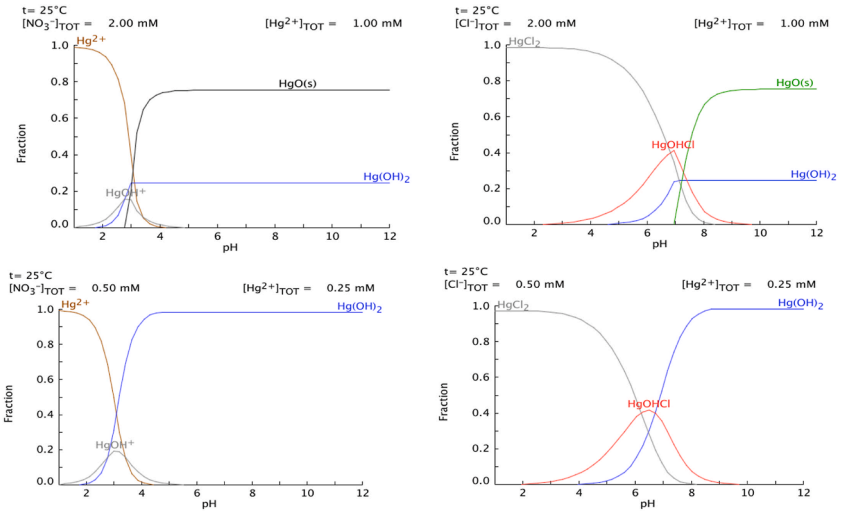

Fig. 10. Speciation diagrams for $Hg(NO_3)_2$ (first/second) and $HgCl_2$ solutions (third/fourth).

In the case of $Hg(NO_3)_2$ solutions the presence of $Ag^+/Ag_2O/Ag^0$ on the surface of the zeolite is not affecting the removal efficiency. This means that considerable amount of exchangeable ions (Na^+, Ag^+) remain on the surface of the zeolite following the modification. Also, under the experimental conditions studied, ion exchange is sufficiently fast and any contribution of amalgamation reaction (4) is insignificant. Taking into account that amalgamation is a slow reaction requiring the reduction followed by diffusion of Hg^0 though the Ag^0/Ag_xHg_y structure (Liu and Huang, 2013) this result is not surprising. In another study, natural and Na^+-exchanged clinoptilolite were used to remove Hg^{2+} from a $Hg(CH_3COO)_2$ solutions (Misaelides and Godelitsas, 1995b). Due to the low initial pH Hg^{2+} was the dominant species, which can be readily be exchanged for Na^+ from the solid phase. However, the addition of the zeolite in the initial solutions causes a pH-increase to 3–4.2 attributed to the simultaneous H^+ uptake. The hydrolysis of Hg^{2+} results in the formation of several ionic species, such as $[Hg(OH)]^+$, $[Hg_2(OH)]^{3+}$, along with neutral $Hg(OH)_2$ complexes. Thus, ion exchange is accompanied by adsorption and surface precipitation of hydrocomplexes.

In $HgCl_2$ solutions and low pH mercury is bounded is the form of neutral $HgCl_2$ complexes and thus ion exchange is not possible unless the $Hg^{2+}\cdots Cl^-$ interactions are disrupted. The performance of Na-NZU in $HgCl_2$ solutions confirms that there is no significant interaction between $HgCl_2$ complexes and the zeolite surface. In the presence of Ag^0 more reactions can take place (Inglezakis et al., 2021b):

$$2Hg^{2+} + 2Ag^0 \rightarrow Hg_2^{2+} + 2Ag^+ \quad (5)$$

$$2Hg_2^{2+} + 2Cl^- \rightarrow Hg_2Cl_2 \quad (6)$$

$$Ag^+ + Cl^- \rightarrow AgCl \quad (7)$$

Although not considered here the amalgamation reactions cannot be excluded. In any case, the precipitation reaction (6) is fast and efficient as is evident by the performance of Ag^0@NZU. This implies that either redox reactions between Ag^0 and $Hg^{2+}\cdots Cl^-$ are possible or these interactions disrupt the complexes making available Hg^{2+}. Also, Ag_2O@NZU and Ag^+@NZU samples remove some mercury, presumably due to some Ag^0 in their structure. XPS analysis of zeolites synthesized by using the same natural sample and similar modifications showed that silver coexists in two oxidation states, i.e. +1 and 0 (Inglezakis et al., 2020c). Due to the complexity of the zeolite XRD spectra the products of these reactions were not identified, however recent research proved the co-existence of amalgams and calomel during the interaction of $HgCl_2$ solution and fumed silica decorated with Ag^0 (Inglezakis et al., 2021b). As the experiments and literature review demonstrate (Table 1) the performance of unmodified zeolites towards the Hg^{2+} removal at low pH and in the presence of Cl^- is poor due to the neutral chlorocomplexes. Nevertheless, in neutral/basic solutions $Hg(OH)_2$ complexes emerge which can be adsorbed or precipitate on zeolites (Fig. 10). For instance, it has been reported that Na-A zeolite (Si/Al ratio of 1) is able to remove Hg^{2+} ions from $HgCl_2$ solutions at pH of 7–7.3 (Hernandez-Tamargo et al., 2021b). The authors provide an explanation based on ion exchange of Hg^{2+} ions and the topology of zeolites framework rather than adsorption or precipitation of hydocomplexes. They argue that Na-A zeolite (LTA framework) has high negative charge density and narrow cage opening of 4 Å which are effective in disrupting the $Hg^{2+}\cdots Cl^-$ interaction, thereby freeing the Hg^{2+} ions and allowing ion exchange to take place. In contrast, zeolite Na–Y (FEU framework type) has lower negative charge density (Si/A ratio of 2–5) and larger cage opening (7 Å) not sufficient to cause $Hg^{2+}\cdots Cl^-$ interaction disruption, thus hindering the ion exchange process. Furthermore, the higher negative charge density of Na-A means stronger electrostatic repulsion of the Cl^- ions. This is in agreement with our experiments as clinoptilolite (HEU framework type) has narrower effective framework pore opening (1.34 × 3.05 × 3.67 Å) than Na-A zeolite but higher Si/Al ratio of 4–6 and thus lower negative charge density resulting to a lower cation exchange capacity (Gili and Conato, 2019). In another study Na-A

and ZSM-5 demonstrated high capacity for Hg^{2+} removal from $HgCl_2$ solutions in a pH range of 2–10 (Alijani et al., 2015b). While the explanation provided above explains the effectiveness of Na-A this is not the case for ZSM-5 (MFI framework), a high silica zeolite (Si/Al typically between 25 and 50) with cage opening of 4.7 × 4.6 × 4.6 Å. The authors argue that the sorption mechanism is a combination of formation of inner sphere complex with Si–O group, ion exchange of $HgOH^+$ and hydrogen bonding. This can explain the effectiveness of ZSM-5 in high pH under the presence of hydrocomplexes and as the experiments showed the sorption is enhanced as pH is increasing. Czarna et al. (2018) studied Na-A, Na-X and Ag^+@Na-X zeolites in $HgCl_2$ solutions. The pH was 5–6 and thus chlorocomplexes predominate. The results showed that the removal efficiency was close to 100% but this is misleading as they used high zeolite mass to solution ratio resulting in low capacity of only 0.12–5.1 mg/g. The zeolites used had a Si/Al ratio of 1.2–1.58 and thus they exhibit high negative charge density, which explains the removal of some Hg^{2+} via ion exchange. The Ag^+@Na-A zeolite had the same performance as the Na-A zeolite, probably due to the absence of Ag^0 explained above. Tauanov et al. (2019) used synthetic sodalite and analcime along with their Ag^0 forms. The performance of Ag^0 zeolites was considerably better than the raw zeolites as a result of the Hg^{2+}-Ag^0 redox reactions. The effect of anions on the removal of Hg^{2+} from aqueous solutions prepared with $HgCl_2$, $Hg(NO_3)_2$, $HgSO_4$ and $Hg(CH_3COO)_2$ was studied for the Ag^0@Sodalite and the results showed that the removal efficiency follows the order: $HgCl_2 > HgSO_4 > Hg(CH_3COO)_2 > Hg(NO_3)_2$. This result can be explained if the zeolite is deprived of all ions during modification in which case, as mentioned above, precipitation reaction (6) in $HgCl_2$ solution is faster than amalgamation reaction (4) that can take place in $Hg(NO_3)_2$ solution.

The mechanisms described above are further corroborated by the iodide removal experiments where the performance of the silver zeolites is reversed, i.e. Ag^+@NZU and Ag_2O@NZU perform better than Ag^0@NZU. The interaction between iodide and silver in aqueous solutions and the formation of KI precipitate on clinoptilolite and other materials is well documented (Inglezakis et al., 2020c; Gradev, 1987; Faghihian et al., 2002; Chmielewská-Horváthová and Lesný, 1995). The samples showed different behavior explained by the reaction mechanism, which favors the Ag^+@NZU and Ag_2O@NZU samples. The surface reactions are (Baimenov et al., 2019):

$$Ag^+ + I^- \rightarrow AgI \tag{9}$$

$$Ag^+ + nI^- + mK^+ \rightarrow [(AgI_n)^{1-n}K^m]^{(m+1)-n} \tag{10}$$

The precipitation reaction (9) and the formation of complexes (10) can take place only under the presence of Ag^+ which implies the oxidation of Ag^0 following reactions (1) and (2) and as a result the iodide removal by Ag^0@NZU is slower.

3.4. Comparison to commercial adsorbents

Particle size is important where it comes to comparison of materials as it affects the kinetics albeit not the equilibrium. The average particle size of the materials used in this study was 1.32 ± 0.03 mm for activated carbon, 1.1 ± 0.3 mm for natural zeolite, 0.81 ± 0.01 mm for cation exchange resin 2.01 ± 0.05 μm for zeolite Y. Based on particle size zeolite Y has an advantage in comparison to the rest of materials as its small size promotes faster kinetics. In Fig. 11 the commercial adsorbents are compared with the best performing materials, i.e. Na-NZU for $Hg(NO_3)_2$ solution and Ag^0@NZU for $HgCl_2$ solution.

The results in $Hg(NO_3)_2$ solutions show that commercial adsorbents exhibit faster kinetics but Na-NZU exhibits higher capacity close to this of activated carbon. As in the case of Na-NZU, in $HgCl_2$ solutions the resin and zeolite Y show no affinity for mercury as expected as all are ion exchange materials while activated carbon and Ag^0@NZU are competing showing similar effectiveness. These results demonstrate that Na-NZU and Ag^0@NZU are effective adsorbents performing better than commercial ion exchangers and are comparable to activated carbon.

4. Conclusions

Different forms of natural zeolite nanocomposites were synthesized with silver content between 55 and 89 mg/g. The nanocomposites were decorated with Ag_m^{n+} clusters and Ag_2O and Ag^0 nanoparticles of size of 4–40 nm. The Na- and Ag-modified materials were used to remove of different forms of mercury from aqueous solutions with an initial concentration of 200 ppm. The study of the removal mechanism is challenging involving mercury aqueous phase speciation and a variety of surface interactions, namely ion exchange, precipitation, amalgamation and red-ox reactions. Removal kinetics, speciation diagrams and several characterizations were used to interpret the phenomena that take place on the surface of the zeolites and a set of probable reactions was provided. Ion exchange was the main mechanism in $Hg(NO_3)_2$ solutions where free Hg^{2+} ions dominate while red-ox reactions and adsorption control the mercury removal in $HgCl_2$ solutions. The zeolites were compared to commercial adsorbents and, under the experimental conditions studied, Na-NZU in $Hg(NO_3)_2$ and Ag^0@NZU in $HgCl_2$ demonstrate comparable effectiveness to this of activated carbon.

Funding

This research has been (partially) funded by the Science Committee of the Ministry of Education and Science of the Republic of Kazakhstan (Grant No. AP14869646).

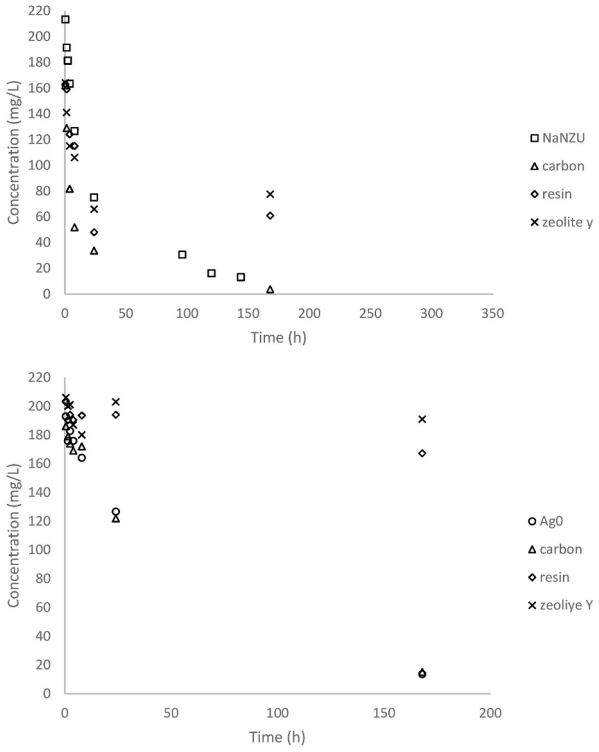

Fig. 11. Residual mercury concentration in $Hg(NO_3)_2$ (upper) and $HgCl_2$ (lower) solutions.

Author statement

V.J.I: Conceptualization, methodology, validation, resources, writing – original draft, supervision, project administration, A.K.: investigation, A.G.: investigation, N.K.: investigation, Z.T.: investigation, writing – original draft, funding.

Declaration of competing interest

The authors declare that they have no known competing financial interests or personal relationships that could have appeared to influence the work reported in this paper.

Data availability

No data was used for the research described in the article.

References

Alijani, H., Beyki, M.H., Mirzababaei, S.N., 2015a. Utilization of synthesized NaA and ZSM-5 nanozeolites for mercury(II) removal: kinetic, thermodynamic and isotherm study. Desalination Water Treat. 55, 1864–1875. https://doi.org/10.1080/19443994.2014.930799.

Alijani, H., Beyki, M.H., Mirzababaei, S.N., 2015b. Utilization of synthesized NaA and ZSM-5 nanozeolites for mercury(II) removal: kinetic, thermodynamic and isotherm study. Desalination Water Treat. 55, 1864–1875. https://doi.org/10.1080/19443994.2014.930799.

Altantzis, T., Coutino-Gonzalez, E., Baekelant, W., Martinez, G.T., Abakumov, A.M., Van Tendeloo, G., Roeffaers, M.B.J., Bals, S., Hofkens, J., 2016a. Direct observation of luminescent silver clusters confined in faujasite zeolites. ACS Nano 10, 7604–7611. https://doi.org/10.1021/acsnano.6b02834.

Altantzis, T., Coutino-Gonzalez, E., Baekelant, W., Martinez, G.T., Abakumov, A.M., Van Tendeloo, G., Roeffaers, M.B.J., Bals, S., Hofkens, J., 2016b. Direct observation of luminescent silver clusters confined in faujasite zeolites. ACS Nano 10, 7604–7611. https://doi.org/10.1021/acsnano.6b02834.

AMAP/UN Environment Expert Group, 2018. Technical Background Report to the Global Mercury Assessment. 2019.

Andrade, Â.L., Cavalcante, L.C.D., Fabris, J.D., Pereira, M.C., Ardisson, J.D., Pizarro, C., 2019. Zeolite-magnetite composites to remove Hg2+ from water. Hyperfine Interact. 240, 18–23. https://doi.org/10.1007/s10751-019-1624-5.

Aspromonte, S.G., Mizrahi, M.D., Schneeberger, F.A., López, J.M.R., Boix, A.V., 2013. Study of the nature and location of silver in Ag-exchanged mordenite catalysts. characterization by spectroscopic techniques. J. Phys. Chem. C 117, 25433–25442. https://doi.org/10.1021/jp4046269.

Attari, M., Bukhari, S.S., Kazemian, H., Rohani, S., 2017. A low-cost adsorbent from coal fly ash for mercury removal from industrial wastewater. J. Environ. Chem. Eng. 5, 391–399. https://doi.org/10.1016/j.jece.2016.12.014.

Azimi, A., Azari, A., Rezakazemi, M., Ansarpour, M., 2017. Removal of heavy metals from industrial wastewaters: a review. ChemBioEng Reviews 4, 37–59. https://doi.org/10.1002/cben.201600010.

Azizi, S.N., Dehnavi, A.R., Joorabdoozha, A., 2013. Synthesis and characterization of LTA nanozeolite using barley husk silica: mercury removal from standard and real solutions. Mater. Res. Bull. 48, 1753–1759. https://doi.org/10.1016/j.materresbull.2012.12.068.

Bahiraei, A., Behin, J., 2020. Sonochemical immobilization of MnO2 nanoparticles on NaP-zeolite for enhanced Hg (II) adsorption from water. J. Environ. Chem. Eng. 8. https://doi.org/10.1016/j.jece.2020.103790.

Baimenov, A.Zh, Berillo, D.A., Inglezakis, V.J., 2019. Cryogel-based Ag°/Ag2O nanocomposites for iodide removal from water. J. Mol. Liq. 299, 112134. https://doi.org/10.1016/j.molliq.2019.112134.

Baimenov, A.Z., Berillo, D.A., Moustakas, K., Inglezakis, V.J., 2020. Efficient removal of mercury (II) from water by use of cryogels and comparison to commercial adsorbents under environmentally relevant conditions. J. Hazard Mater. 399, 123056. https://doi.org/10.1016/j.jhazmat.2020.123056.
Beckers, F., Rinklebe, J., 2017a. Cycling of mercury in the environment: sources, fate, and human health implications: a review. Crit. Rev. Environ. Sci. Technol. 47, 693–794. https://doi.org/10.1080/10643389.2017.1326277.
Beckers, F., Rinklebe, J., 2017b. Cycling of mercury in the environment: sources, fate, and human health implications: a review. Crit. Rev. Environ. Sci. Technol. 47, 693–794. https://doi.org/10.1080/10643389.2017.1326277.
Campbell, L.S., Chimedtsogzol, A., Dyer, A., 2006a. Species sensitivity of zeolite minerals for uptake of mercury solutes. Mineral. Mag. 70, 361–371. https://doi.org/10.1180/0026461067040341.
Campbell, L.S., Chimedtsogzol, A., Dyer, A., 2006b. Species sensitivity of zeolite minerals for uptake of mercury solutes. Mineral. Mag. 70, 361–371. https://doi.org/10.1180/0026461067040341.
Chebbi, M., Azambre, B., Cantrel, L., Huvé, M., Albiol, T., 2017. Influence of structural, textural and chemical parameters of silver zeolites on the retention of methyl iodide. Microporous Mesoporous Mater. 244, 137–150. https://doi.org/10.1016/j.micromeso.2017.02.056.
Chmielewská-Horváthová, E., Lesný, J., 1995. Iodide adsorption on the surface of chemically pretreated clinoptilolite. J. Radioanalytical. Nuclear Chem. Lett. 200, 351–363. https://doi.org/10.1007/BF02163788.
Chojnacki, A., Chojnacka, K., Hoffmann, J., Górecki, H., 2004. The application of natural zeolites for mercury removal: from laboratory tests to industrial scale. Miner. Eng. 17, 933–937. https://doi.org/10.1016/j.mineng.2004.03.002.
Coutiño-Gonzalez, E., Baekelant, W., Steele, J.A., Kim, C.W., Roeffaers, M.B.J., Hofkens, J., 2017a. Silver clusters in zeolites: from self-assembly to ground-breaking luminescent properties. Acc. Chem. Res. 50, 2353–2361. https://doi.org/10.1021/acs.accounts.7b00295.
Coutiño-Gonzalez, E., Baekelant, W., Steele, J.A., Kim, C.W., Roeffaers, M.B.J., Hofkens, J., 2017b. Silver clusters in zeolites: from self-assembly to ground-breaking luminescent properties. Acc. Chem. Res. 50, 2353–2361. https://doi.org/10.1021/acs.accounts.7b00295.
Crockett, M.P., Evans, A.M., Worthington, M.J.H., Albuquerque, I.S., Slattery, A.D., Gibson, C.T., Campbell, J.A., Lewis, D.A., Bernardes, G.J.L., Chalker, J.M., 2016. Sulfur-limonene polysulfide: a material synthesized entirely from industrial by-products and its use in removing toxic metals from water and soil. Angew. Chem. Int. Ed. 55, 1714–1718. https://doi.org/10.1002/anie.201508708.
Czarna, D., Baran, P., Kunecki, P., Panek, R., Żmuda, R., Wdowin, M., 2018. Synthetic zeolites as potential sorbents of mercury from wastewater occurring during wet FGD processes of flue gas. J. Clean. Prod. 172, 2636–2645. https://doi.org/10.1016/j.jclepro.2017.11.147.
De Clercq, J., 2012. Removal of Mercury from Aqueous Solutions by Adsorption on a New Ultra Stable Mesoporous Adsorbent and on a Commercial Ion Exchange Resin. pp. 6–11.
De Cremer, G., Coutiño-Gonzalez, E., Roeffaers, M.B.J., Moens, B., Ollevier, J., Van Der Auweraer, M., Schoonheydt, R., Jacobs, P.A., De Schryver, F.C., Hofkens, J., De Vos, D.E., Sels, B.F., Vosch, T., 2009a. Characterization of fluorescence in heat-treated silver-exchanged zeolites. J. Am. Chem. Soc. 131, 3049–3056. https://doi.org/10.1021/ja810071s.
De Cremer, G., Coutiño-Gonzalez, E., Roeffaers, M.B.J., Moens, B., Ollevier, J., Van Der Auweraer, M., Schoonheydt, R., Jacobs, P.A., De Schryver, F.C., Hofkens, J., De Vos, D.E., Sels, B.F., Vosch, T., 2009b. Characterization of fluorescence in heat-treated silver-exchanged zeolites. J. Am. Chem. Soc. 131, 3049–3056. https://doi.org/10.1021/ja810071s.
El-Roz, M., Telegeiev, I., Mordvinova, N.E., Lebedev, O.I., Barrier, N., Behilil, A., Zaarour, M., Lakiss, L., Valtchev, V., 2018. Uniform generation of sub-nanometer silver clusters in zeolite cages exhibiting high photocatalytic activity under visible light. ACS Appl. Mater. Interfaces 10, 28702–28708. https://doi.org/10.1021/acsami.8b09634.
Esdaile, L.J., Chalker, J.M., 2018. The mercury problem in artisanal and small-scale gold mining. Chem. Eur J. 24, 6905–6916. https://doi.org/10.1002/chem.201704840.
Faghihian, H., Maragheh, M.G., Malekpour, A., 2002. Adsorption of radioactive iodide by natural zeolites. J. Radioanal. Nucl. Chem. 254, 545–550. https://doi.org/10.1023/A:1021698207045.
Fang, R., Lu, C., Zhang, W., Xiao, Z., Chen, H., Liang, C., Huang, H., Gan, Y., Zhang, J., Xia, Y., 2018. Supercritical CO2 assisted synthesis of sulfur-modified zeolites as high-efficiency adsorbents for Hg2+ removal from water. New J. Chem. 42, 3541–3550. https://doi.org/10.1039/c7nj04869f.
Fardmousavi, O., Faghihian, H., 2014. Thiol-functionalized hierarchical zeolite nanocomposite for adsorption of Hg2+from aqueous solutions. Compt. Rendus Chem. 17, 1203–1211. https://doi.org/10.1016/j.crci.2014.05.001.
Flores-López, N.S., Castro-Rosas, J., Ramírez-Bon, R., Mendoza-Córdova, A., Larios-Rodríguez, E., Flores-Acosta, M., 2012. Synthesis and properties of crystalline silver nanoparticles supported in natural zeolite chabazite. J. Mol. Struct. 1028, 110–115. https://doi.org/10.1016/j.molstruc.2012.05.080.
Ge, H., Hua, T., 2016. Synthesis and characterization of poly(maleic acid)-grafted crosslinked chitosan nanomaterial with high uptake and selectivity for Hg(II) sorption. Carbohydr. Polym. 153, 246–252. https://doi.org/10.1016/j.carbpol.2016.07.110.
Gili, M.B.Z., Conato, M.T., 2019. Adsorption uptake of mordenite-type zeolites with varying si/al ratio on zn2+ ions in aqueous solution. Mater. Res. Express 6. https://doi.org/10.1088/2053-1591/aafc08.
Golubeva, O.Y., Ul'yanova, N.Y., 2015. Stabilization of silver nanoparticles and clusters in porous zeolite matrices with Rho, Beta, and paulingite structures. Glass Phys. Chem. 41, 537–544. https://doi.org/10.1134/S1087659615050065.
Gradev, G.D., 1987. Sorption of iodide ions on cationic forms of clinoptilolite. J. Radioanalytical. Nuclear Chem. Articles. 116, 341–346. https://doi.org/10.1007/BF02035778.
Gurin, V.S., Petranovskii, V.P., Hernandez, M.A., Bogdanchikova, N.E., Alexeenko, A.A., 2005. Silver and copper clusters and small particles stabilized within nanoporous silicate-based materials. Mater. Sci. Eng. 391, 71–76. https://doi.org/10.1016/j.msea.2004.08.054.
Gworek, B., Bemowska-Kałabun, O., Kijeńska, M., Wrzosek-Jakubowska, J., 2016. Mercury in marine and oceanic waters---a review. Water Air Soil Pollut. 227, 371. https://doi.org/10.1007/s11270-016-3060-3.
Hernandez-Tamargo, C., Kwakye-Awuah, B., O'Malley, A.J., de Leeuw, N.H., 2021a. Mercury exchange in zeolites Na-A and Na-Y studied by classical molecular dynamics simulations and ion exchange experiments. Microporous Mesoporous Mater. 315, 110903. https://doi.org/10.1016/j.micromeso.2021.110903.
Hernandez-Tamargo, C., Kwakye-Awuah, B., O'Malley, A.J., de Leeuw, N.H., 2021b. Mercury exchange in zeolites Na-A and Na-Y studied by classical molecular dynamics simulations and ion exchange experiments. Microporous Mesoporous Mater. 315, 110903. https://doi.org/10.1016/j.micromeso.2021.110903.
Inglezakis, V.J., Loizidou, M.D., Grigoropoulou, H.P., 2002. Equilibrium and kinetic ion exchange studies of Pb2+, Cr3+, Fe3+ and Cu2+ on natural clinoptilolite. Water Res. 36, 2784–2792. https://doi.org/10.1016/S0043-1354(01)00504-8.
Inglezakis, V.J., Satayeva, A., Yagofarova, A., Tauanov, Z., Meiramkulova, K., Farrando-Pérez, J., Bear, J.C., 2020a. Surface interactions and mechanisms study on the removal of iodide from water by use of natural Zeolite-based silver nanocomposites. Nanomaterials 10, 1–23. https://doi.org/10.3390/nano10061156.
Inglezakis, V.J., Satayeva, A., Yagofarova, A., Tauanov, Z., Meiramkulova, K., Farrando-Pérez, J., Bear, J.C., 2020b. Surface interactions and mechanisms study on the removal of iodide from water by use of natural Zeolite-based silver nanocomposites. Nanomaterials 10, 1–23. https://doi.org/10.3390/nano10061156.
Inglezakis, V.J., Satayeva, A., Yagofarova, A., Tauanov, Z., Meiramkulova, K., Farrando-Pérez, J., Bear, J.C., 2020c. Surface interactions and mechanisms study on the removal of iodide from water by use of natural Zeolite-based silver nanocomposites. Nanomaterials 10, 1–23. https://doi.org/10.3390/nano10061156.
Inglezakis, V.J., Azat, S., Tauanov, Z., Mikhalovsky, S.V., 2021a. Functionalization of biosourced silica and surface reactions with mercury in aqueous solutions. Chem. Eng. J. 423, 129745. https://doi.org/10.1016/j.cej.2021.129745.
Inglezakis, V.J., Azat, S., Tauanov, Z., Mikhalovsky, S.V., 2021b. Functionalization of biosourced silica and surface reactions with mercury in aqueous solutions. Chem. Eng. J. 423, 129745. https://doi.org/10.1016/j.cej.2021.129745.
Kabiri, S., Tran, D.N.H., Azari, S., Losic, D., 2015. Graphene-diatom silica aerogels for efficient removal of mercury ions from water. ACS Appl. Mater. Interfaces 7, 11815–11823. https://doi.org/10.1021/acsami.5b01159.
Kamensky, O.L., Horton, D., Kingsley, D.P., Bridges, C.C., 2019. A case of accidental mercury intoxication. J. Emerg. Med. 56, 275–278. https://doi.org/10.1016/j.jemermed.2018.12.039.
Kuntubek, A., Kinayat, N., Meiramkulova, K., Poulopoulos, S., Bear, J.C., Inglezakis, V.J., 2020. Catalytic oxidation of methylene blue by use of natural zeolite-based silver and magnetite nanocomposites. Processes 8, 471. https://doi.org/10.3390/pr8040471.

Li, Y., Yang, L., Li, X., Miki, T., Nagasaka, T., 2021. A composite adsorbent of ZnS nanoclusters grown in zeolite NaA synthesized from fly ash with a high mercury ion removal efficiency in solution. J. Hazard Mater. 411. https://doi.org/10.1016/j.jhazmat.2021.125044.
Lihareva, N., Dimova, L., Petrov, O., Tzvetanova, Y., 2010. Ag+ sorption on natural and Na-exchanged clinoptilolite from Eastern Rhodopes, Bulgaria. Microporous Mesoporous Mater. 130, 32–37. https://doi.org/10.1016/j.micromeso.2009.10.009.
Liu, Y., Huang, C.Z., 2013. Real-time dark-field scattering microscopic monitoring of the in situ growth of single ag@hg nanoalloys. ACS Nano 7, 11026–11034. https://doi.org/10.1021/nn404694e.
Liu, Y., Zhu, Z., Liu, G., Xu, Z., Kuznicki, S.M., Zhang, H., 2011. A novel method to improve crystallinity of supported nanoparticles using low melting point metals. J. Phys. Chem. C 115, 14591–14597. https://doi.org/10.1021/jp203155z.
Liu, J., Huang, H., Huang, R., Zhang, J., Hao, S., Shen, Y., Chen, H., 2016. Mechanisms of CPB modified zeolite on mercury adsorption in simulated wastewater. Water Environ. Res. 88, 490–499. https://doi.org/10.2175/106143016x14504669767850.
Misaelides, P., Godelitsas, A., 1995a. Removal of heavy metals from aqueous solutions using pretreated natural zeolitic materials: the case of mercury(II). Toxicol. Environ. Chem. 51, 21–29. https://doi.org/10.1080/02772249509358223.
Misaelides, P., Godelitsas, A., 1995b. Removal of heavy metals from aqueous solutions using pretreated natural zeolitic materials: the case of mercury(II). Toxicol. Environ. Chem. 51, 21–29. https://doi.org/10.1080/02772249509358223.
Moshoeshoe, M., Silas Nadiye-Tabbiruka, M., Obuseng, V., 2017. A review of the chemistry, structure, properties and applications of zeolites. Am. J. Mater. Sci. 2017, 196–221. https://doi.org/10.5923/j.materials.20170705.12.
Mudasir, M., Karelius, K., Aprilita, N.H., Wahyuni, E.T., 2016. Adsorption of mercury(II) on dithizone-immobilized natural zeolite. J. Environ. Chem. Eng. 4, 1839–1849. https://doi.org/10.1016/j.jece.2016.03.016.
Mulfinger, L., Solomon, S.D., Bahadory, M., v Jeyarajasingam, A., Rutkowsky, S.A., Boritz, C., 2007. Synthesis and study of silver nanoparticles. J Chem. Educ. 84, 322. https://doi.org/10.1021/ed084p322.
Murthy, Z.V.P., Parikh, P.A., Patel, N.B., 2013. Application of β-zeolite, zeolite Y, and mordenite as adsorbents to remove mercury from aqueous solutions. J. Dispersion Sci. Technol. 34, 747–755. https://doi.org/10.1080/01932691.2012.685839.
Oliveira, J.R., Vasques, I.C.F., Lima, F.R.D., Carvalho, G.S., Job, M.T.P., de Oliveira, T.S., Marques, J.J., 2020. Mercury adsorption in tropical soils and zeolite: characterization by Fourier-transform infrared spectroscopy. Arch. Agron Soil Sci. 1–16. https://doi.org/10.1080/03650340.2020.1845318. 00. .
Prasetya, A., Prihutami, P., Warisaura, A.D., Fahrurrozi, M., Murti Petrus, H.T.B., 2020. Characteristic of Hg removal using zeolite adsorption and Echinodorus palaefolius phytoremediation in subsurface flow constructed wetland (SSF-CW) model. J. Environ. Chem. Eng. 8, 103781. https://doi.org/10.1016/j.jece.2020.103781.
Qu, Z., Fang, L., Chen, D., Xu, H., Yan, N., 2017. Effective and regenerable Ag/graphene adsorbent for Hg(II) removal from aqueous solution. Fuel 203, 128–134. https://doi.org/10.1016/j.fuel.2017.04.105.
Saha, D., Barakat, S., Van Bramer, S.E., Nelson, K.A., Hensley, D.K., Chen, J., 2016. Noncompetitive and competitive adsorption of heavy metals in sulfur-functionalized ordered mesoporous carbon. ACS Appl. Mater. Interfaces 8, 34132–34142. https://doi.org/10.1021/acsami.6b12190.
Salam, M.A., Abukhadra, M.R., Mostafa, M., 2020. Effective decontamination of As(V), Hg(II), and U(VI) toxic ions from water using novel muscovite/zeolite aluminosilicate composite: adsorption behavior and mechanism. Environ. Sci. Pollut. Control Ser. 27, 13247–13260. https://doi.org/10.1007/s11356-020-07945-8.
Sánchez-Hernández, R., Padilla, I., López-Andrés, S., López-Delgado, A., 2018. Single and competitive adsorptive removal of lead, cadmium, and mercury using zeolite adsorbent prepared from industrial aluminum waste. Desalination Water Treat. 126, 181–195. https://doi.org/10.5004/dwt.2018.22816.
Shirzadi, H., Nezamzadeh-Ejhieh, A., 2017. An efficient modified zeolite for simultaneous removal of Pb(II) and Hg(II) from aqueous solution. J. Mol. Liq. 230, 221–229. https://doi.org/10.1016/j.molliq.2017.01.029.
Siva, S., Sudharsan, S., Sayee Kannan, R., 2015. Synthesis, characterization and ion-exchange properties of novel hybrid polymer nanocomposites for selective and effective mercury(ii) removal. RSC Adv. 5, 79665–79678. https://doi.org/10.1039/C5RA13004B.
Somerset, V., Petrik, L., Iwuoha, E., 2008. Alkaline hydrothermal conversion of fly ash precipitates into zeolites 3: the removal of mercury and lead ions from wastewater. J. Environ. Manag. 87, 125–131. https://doi.org/10.1016/j.jenvman.2007.01.033.
Stylianou, M., Inglezakis, V., Agapiou, A., Itskos, G., Jetybayeva, A., Loizidou, M., 2018a. A comparative study on phyllosilicate and tectosillicate mineral structural properties. Desalination Water Treat. 112, 119–146. https://doi.org/10.5004/dwt.2018.21968.
Stylianou, M., Inglezakis, V., Agapiou, A., Itskos, G., Jetybayeva, A., Loizidou, M., 2018b. A comparative study on phyllosilicate and tectosillicate mineral structural properties. Desalination Water Treat. 112, 119–146. https://doi.org/10.5004/dwt.2018.21968.
Stylianou, M., Inglezakis, V., Agapiou, A., Itskos, G., Jetybayeva, A., Loizidou, M., 2018c. A comparative study on phyllosilicate and tectosillicate mineral structural properties. Desalination Water Treat. 112, 119–146. https://doi.org/10.5004/dwt.2018.21968.
Sumesh, E., Bootharaju, M.S., Anshup, Pradeep, T., 2011. A practical silver nanoparticle-based adsorbent for the removal of Hg2+ from water. J. Hazard Mater. 189, 450–457. https://doi.org/10.1016/j.jhazmat.2011.02.061.
Taiji, K., Iso, Y., Isobe, T., 2018. Fluorescent Ag+-exchanged zeolite nanoparticles with improved photoluminescence properties via X-ray irradiation. J. Lumin. 196, 214–220. https://doi.org/10.1016/j.jlumin.2017.12.028.
Tarach, K., Góra-Marek, K., Chrzan, M., Walas, S., 2014. Quantification of silver sites in zeolites: carbon monoxide sorption monitored by IR spectroscopy. J. Phys. Chem. C 118, 23751–23760. https://doi.org/10.1021/jp506820v.
Tauanov, Z., Tsakiridis, P.E., Mikhalovsky, S.V., Inglezakis, V.J., 2018. Synthetic coal fly ash-derived zeolites doped with silver nanoparticles for mercury (II) removal from water. J. Environ. Manag. 224, 164–171. https://doi.org/10.1016/j.jenvman.2018.07.049.
Tauanov, Z., Tsakiridis, P.E., Shah, D., Inglezakis, V.J., 2019. Synthetic sodalite doped with silver nanoparticles: characterization and mercury (II) removal from aqueous solutions. J. Environ. Sci. Health, Part A. 1–9. https://doi.org/10.1080/10934529.2019.1611129.
Tauanov, Z., Lee, J., Inglezakis, V.J., 2020. Mercury reduction and chemisorption on the surface of synthetic zeolite silver nanocomposites: equilibrium studies and mechanisms. J. Mol. Liq. 305, 112825. https://doi.org/10.1016/j.molliq.2020.112825.
Tikoalu, A.D., Lundquist, N.A., Chalker, J.M., 2020. Mercury sorbents made by inverse vulcanization of sustainable triglycerides: the plant oil structure influences the rate of mercury removal from water. Adv Sustain Syst 4, 1900111. https://doi.org/10.1002/adsu.201900111.
Ugrina, M., Čeru, T., Nuić, I., Trgo, M., 2020. Comparative study of mercury(Ii) removal from aqueous solutions onto natural and iron-modified clinoptilolite rich zeolite. Processes 8, 1–21. https://doi.org/10.3390/pr8111523.
Wang, X., Sun, R., Wang, C., 2014. pH dependence and thermodynamics of Hg(II) adsorption onto chitosan-poly(vinyl alcohol) hydrogel adsorbent. Colloids Surf. A Physicochem. Eng. Asp. 441, 51–58. https://doi.org/10.1016/j.colsurfa.2013.08.068.
Wang, L., Hou, D., Cao, Y., Ok, Y.S., Tack, F.M.G.G., Rinklebe, J., O'Connor, D., 2020a. Remediation of mercury contaminated soil, water, and air: a review of emerging materials and innovative technologies. Environ. Int. 134, 105281. https://doi.org/10.1016/j.envint.2019.105281.
Wang, L., Hou, D., Cao, Y., Ok, Y.S., Tack, F.M.G.G., Rinklebe, J., O'Connor, D., 2020b. Remediation of mercury contaminated soil, water, and air: a review of emerging materials and innovative technologies. Environ. Int. 134, 105281. https://doi.org/10.1016/j.envint.2019.105281.
Yorifuji, T., Tsuda, T., Kashima, S., Takao, S., Harada, M., 2010. Long-term exposure to methylmercury and its effects on hypertension in Minamata. Environ. Res. 110, 40–46. https://doi.org/10.1016/j.envres.2009.10.011.
Yorifuji, T., Tsuda, T., Inoue, S., Takao, S., Harada, M., 2011. Long-term exposure to methylmercury and psychiatric symptoms in residents of Minamata, Japan. Environ. Int. 37, 907–913. https://doi.org/10.1016/j.envint.2011.03.008.
Yu, F., Chen, Y., Wang, Y., Liu, C., Ma, W., 2018. Enhanced removal of iodide from aqueous solution by ozonation and subsequent adsorption on Ag-Ag2O modified on Carbon Spheres. Appl. Surf. Sci. 427, 753–762. https://doi.org/10.1016/j.apsusc.2017.08.089.